

AERODYNAMIC DEFORMATION EXPERIMENT OF SERPENTINE NOZZLE FOR TURBOFAN AND ANALYSIS OF FLUID-STRUCTURE INTERACTION METHOD

Qiulin Li¹, Li Zhou^{1,2}, Zhanxue Wang¹, Xiaobo Zhang¹, Sheng Huang¹

1.School of Power and Energy, Northwestern Polytechnical University, Xi'an, 710072, China 2.Collaborative Innovation Center for Advanced Aero-Engine, Beijing, 100191, China

Abstract

The serpentine nozzle is a crucial component in stealth aircraft for reducing detectable signals. This paper compares the aerodynamic-deformation coupling characteristics of the serpentine nozzle under unidirectional and bidirectional fluid-structure interaction (FSI) methods and verifies the accuracy of different coupling methods through experimental research. The results indicate that the deformation distribution trends of the serpentine nozzle are consistent under both unidirectional and bidirectional FSI methods. However, the overall deformation is greater with the unidirectional coupling method, with a maximum deformation of 32.2 mm compared to 27.6 mm for the bidirectional coupling method. The aerodynamic performance of the serpentine nozzle decreases after undergoing FSI, with the total pressure recovery coefficient reduced by 1.2% and the thrust coefficient reduced by 0.5% under unidirectional coupling. Under bidirectional coupling, the total pressure recovery coefficient is reduced by 1.1% and the thrust coefficient by 1.75%. Based on experimental and numerical studies, the maximum error for the unidirectional FSI method is 23.4%, while for the bidirectional FSI method, it is 9.1%. The bidirectional coupling method can accurately simulate the aerodynamic deformation characteristics of the serpentine nozzle in turbofan engines, aligning more closely with physical laws under real-world conditions.

Keywords: Serpentine nozzle; Experimental research; Deformation characteristics; Fluid-structure interaction

1. Introduction

In modern warfare, to evade precision-guided weapons, stealth capability has become essential for next-generation fighter jets. The low-observable serpentine stealth nozzle is a critical technology for enhancing the stealth performance of aircraft engine exhaust systems. Due to the serpentine nozzle's high-curvature, complex flow path, and thin-walled structure, as well as its operation in high-pressure and high-temperature environments, significant structural deformations and even localized tearing have become major bottlenecks in its application on stealth aircraft [1,2]. The unique configuration of the serpentine nozzle results in continuous interaction between the internal flow field and the structure, leading to stress concentration and significant structural deformations, as well as complex aeroelastic phenomena [3,4]. This strong fluid-structure interaction significantly alters the nozzle's aerodynamic characteristics, affecting its operational state and causing potentially severe damage to combat aircraft [5,6]. Therefore, it is necessary to conduct numerical and experimental studies on the aerodynamic deformation mechanism and computational methods of the serpentine nozzle.

Fluid-structure interaction (FSI) methods can be classified into unidirectional and bidirectional coupling based on data transfer mechanisms. Unidirectional coupling involves one-way data transfer between the fluid and structural domains at the coupling interface, resulting in faster computation but lower accuracy. Bidirectional coupling involves mutual data transfer and feedback between the fluid and structural domains at the coupling interface. Although bidirectional coupling requires more computational resources, it more accurately reflects the essence of fluid-structure interaction and provides higher computational accuracy [7,8]. In current multiphysics coupling studies of exhaust

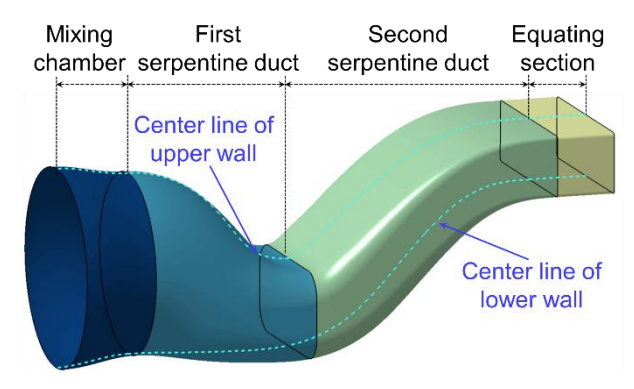
systems, Urbanczyk and Alonso [9] developed a multiphysics analysis and design optimization software, COMANDO, using a unidirectional fluid-structure interaction method to optimize the wall thickness of supersonic two-dimensional nozzles. Nigam and Sricharan [10] conducted unidirectional fluid-thermal interaction studies on axisymmetric exhaust system composite structures, comparing the effects of pressure loads and thermal loads on structural deformation characteristics. Smith [11] investigated deformation suppression methods for the serpentine nozzle equipped on the "Eikon" stealth UAV using a bidirectional coupling method. Sun Peng [12] analyzed the aerodynamic performance changes of serpentine nozzle with different thicknesses before and after fluid-structure interaction using a bidirectional fluid-structure interaction method. The results indicate that as the wall thickness increases from 3mm to 6mm, the maximum deformation displacement of the serpentine nozzle decreases by 68.5mm. Compared to the uncoupled state, the variation in axial thrust decreases from 2.70% to 0.70% in the coupled state. For the serpentine nozzle, a component with a complex flow field and thin-walled structure, current research has not considered the impact of different temporal coupling mechanisms on its structural deformation and aerodynamic performance. There is also a lack of experimental research on the FSI methods and deformation mechanisms of the serpentine nozzle.

In summary, the numerical methods and experimental studies on the FSI of serpentine nozzles are not yet covered in the literature. Investigating the aerodynamic deformation under FSI and selecting suitable computational methods are crucial for obtaining high aerodynamic performance and strong structural stability in practical engineering applications. Therefore, this paper conducts experimental research on the structural deformation of the serpentine nozzle and compares the aerodynamic performance and structural deformation characteristics under unidirectional and bidirectional FSI computations. It also verifies the reliability of different FSI algorithms through experiments to obtain an FSI computational method for serpentine nozzles that aligns more closely with physical laws under real conditions.

2. Geometry of exhaust system

The research object of this paper is a double-annular serpentine nozzle based on a certain type of mixed-flow turbofan engine, as shown in Figure 1. The exhaust mixer comes from the end structure of the turbofan engine, and the outlet area of the serpentine nozzle is obtained by calculating the overall performance of the engine. The serpentine nozzle achieves the improvement of infrared stealth capability by blocking the high-temperature components of the engine through profile, and this paper designs different configurations of serpentine nozzle based on the variable cross-section design method with multi-parameter coupling, through the design of nozzle centerline change rule, nozzle flow cross-section design along the path, and establishment of low observable design criteria. The three-dimensional centerline design of the serpentine nozzle is mainly based on the extension of the two-dimensional Lee curve method [13] in three-dimensional space, to meet the three-dimensional spatial attribute requirements of nozzle inlet/outlet position, and make the geometric configuration of the nozzle better layout in the limited space inside the fuselage. The establishment of low observable design criteria is achieved by completely blocking the high-temperature components of the engine by serpentine profile, so that it is impossible to detect high-temperature components at any detection angle, and reduce infrared radiation intensity.

Figure 2 shows a schematic diagram of key geometric parameters of S-bend section, where nozzle inlet area is determined by mixer outlet diameter, and nozzle outlet area is determined by engine performance parameters. The main design parameters of serpentine nozzle include nozzle diameter (D), nozzle length (L), first bend channel axial length (L_1) , first bend longitudinal offset $(\Delta Y_1/L_1)$, second bend channel axial length (L_2) , second bend longitudinal offset $(\Delta Y_2/L_2)$, nozzle exit aspect ratio (W_0/H_0) , equal straight section length (L_3) . L_1 and L_2 are dimensionless as second bend to first bend length ratio (L_2/L_1) , and L_3 is dimensionless as equal straight section length to diameter ratio (L_3/D) . The values of dimensionless parameters formed by key geometric parameter combination under design state are shown in Table 1.



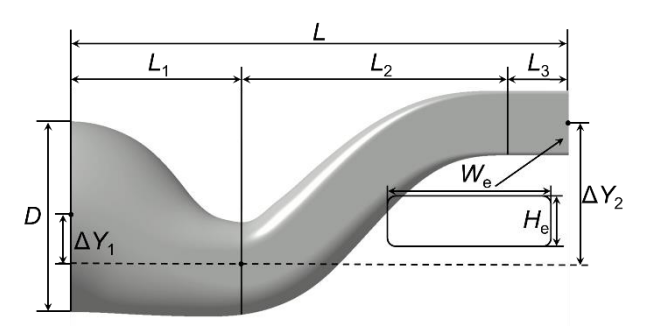


Figure 1 – Geometry model of double serpentine nozzle.

Figure 2 – Design parameters of double serpentine nozzle.

Table 1. Design parameters of serpentine nozzle.

Geometric parameter	Numerical value		
Nozzle length-L(mm)	2098.2		
Nozzle diameter-D(mm)	807		
Second bend/first bend length ratio-L ₂ /L ₁	1.5		
First turn longitudinal deflection-ΔY ₁ /L ₁	-0.3		
Second bend longitudinal deflection-ΔY ₂ /L ₂	0.36		
Nozzle exit aspect ratio-W _e /H _e	3		

Figure 3 illustrates the low observability design criteria for the serpentine nozzle that completely shields high-temperature components. The serpentine nozzle achieves full concealment of the mixing chamber when the points M (the tangent point of the upper longitudinal line on the symmetry plane of the nozzle), N (the tangent point of the lower longitudinal line), and B (the top vertex of the nozzle exit) are collinear, or when points M, N, and A (the lower vertex at the end of the thermal component) are collinear. The shaded area in the figure represents the visible range of infrared detection. For longitudinally deflected double serpentine nozzle, if the axial length of the nozzle is relatively short, the second bend's longitudinal offset first meets the collinearity constraint of points M, N, and B. If the axial length of the nozzle is relatively long, the second bend's longitudinal offset first meets the collinearity constraint of points M, N, and A. The S-bend nozzle configuration designed in this study satisfies the collinearity constraint of M, N, and B.

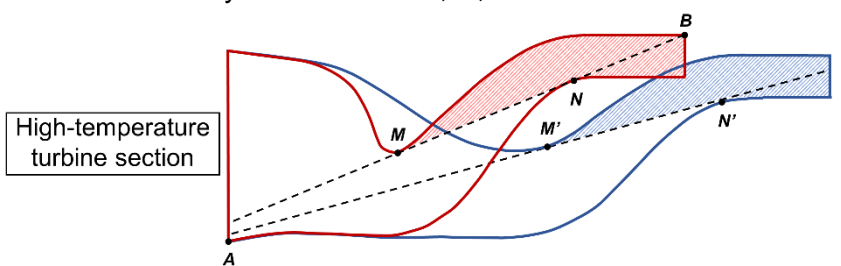


Figure 3 – Criterions to completely shield high temperature.

The schematic diagram of the fluid-structure interaction model for the serpentine nozzle is shown in Figure 4. In this model, the internal flow of the nozzle is the engine exhaust, while the external flow is the atmospheric free stream. The coupling surface consists of the inner wall, outer wall, and exit wall of the nozzle. The aerodynamic load F and the deformation displacement U are synchronously exchanged on the coupling surface. The specific coupling process is as follows: The drastic changes in the aerodynamic load F generated by the internal flow field of the serpentine nozzle are applied to the structural surface through the coupling surface, resulting in complex structural deformation characteristics. The deformation displacement U of the nozzle structure, in turn, acts on the inner and outer flow field boundaries through the coupling surface, affecting the internal and external flow characteristics of the nozzle and altering the distribution of aerodynamic loads on the wall surfaces.

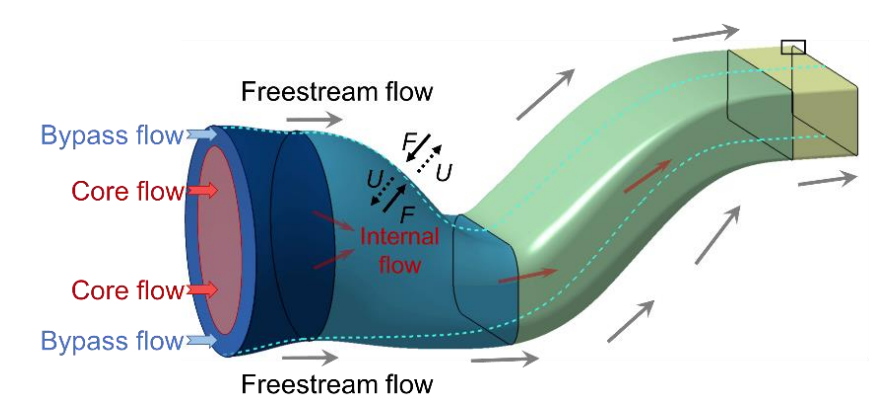


Figure 4 – Fluid-structure interaction model of serpentine nozzle.

3. Numerical method and coupled solution method

3.1 Numerical methods and verification

Numerical simulation of the fluid domain of the serpentine nozzle is conducted using Computational Fluid Dynamics (CFD) software Fluent. The three-dimensional unsteady compressible Reynolds-averaged Navier-Stokes (N-S) equations are solved using a pressure-based approach, with the SST k- ω turbulence model employed. Second-order upwind discretization is used for spatial discretization, with the working fluid assumed to be an ideal gas. The solid domain of the serpentine nozzle is analyzed using Computational structural dynamics (CSD) software Abaqus. Finite element method is utilized for structural analysis, and the Newmark- β direct integration method is employed for solving the structural dynamic equations in the time domain. Dynamic implicit analysis steps are utilized.

The entire three-dimensional flow field of the dual-duct serpentine nozzle is meshed using ICEM software, with a mixed mesh comprising the nozzle domain and the far-field domain. The nozzle structure deformation leads to continuous movement of the flow field boundaries, hence the nozzle domain is set as dynamic and tetrahedral unstructured mesh is employed, with mesh smoothing and reconstruction to adapt to the evolving flow field. To prevent negative volumes due to excessive grid deformation during coupling, dynamic mesh techniques are used to adjust grid motion within the boundary layer, maintaining relative motionlessness of boundary layer grids with respect to the wall. The far-field domain is set as static and hexahedral structured mesh is used, with no deformation or reconstruction of the mesh in this region. An interior is defined between the dynamic nozzle domain and the static far-field domain. The flow field computation domain is discretized using second-order upwind scheme, with an ideal gas assumption, and Roe-FDS scheme is used for discretizing convective fluxes. After grid independence verification, the mesh used for computation consists of 5.38 million elements. The mesh and boundary conditions for the fluid domain are shown in Figure 5. The inlet boundaries for the inner and outer ducts are set as pressure inlet boundary conditions, with specific conditions listed in Table 2. The incoming flow at the inlets is aligned in the axial direction, and the nozzle exit back pressure is set to 1 atm.

The structural domain of the dual-duct serpentine nozzle is meshed using hexahedral elements, with C3D8I hexahedral elements as the mesh unit type. The serpentine nozzle is assumed to be a cantilever beam structure, with fixed boundary constraint applied at the inlet face and a wall thickness of 5mm. The structural material selected is a 706 high-temperature alloy assumed to be isotropic, with material properties including elastic modulus, density, and Poisson's ratio, with specific parameter values as shown in Table 3. Rayleigh damping assumption is applied to the nozzle structure, with damping coefficient η = 78.49 and α = 1.2516e-2. The effects of nozzle structure gravity and heat flux exchange are neglected. After grid independence verification, the mesh quantity used for computation consists of 80,664 elements. The grid for the solid domain is shown in Figure

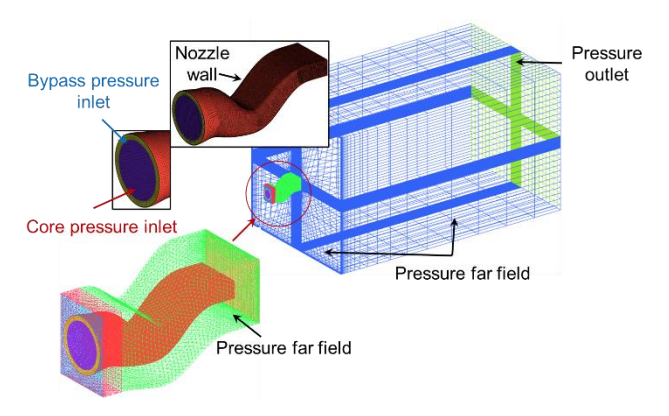
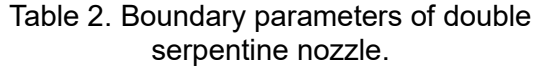


Figure 5 – Numerical grid and boundary condition.



Position	Internal channel inlet	Outside bypass inlet		
P*(atm)	1.54	1.60		
<i>T</i> (K)	987.15	412.70		

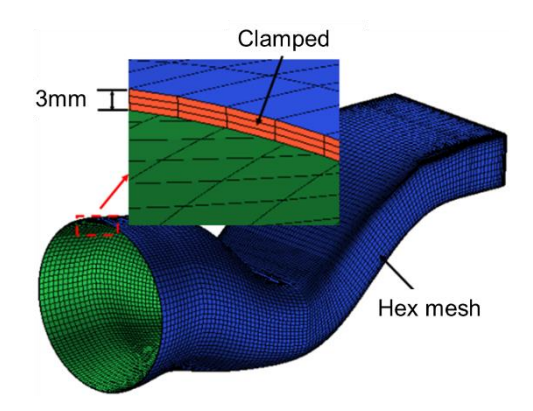


Figure 6 – Finite element model of the solid domain.

Table 3. The physical properties of solid material.

Material parameter	Value
Elastic Modulus-E(GPa)	210
Density- ρ (kg/m³)	8100
Poisson's ratio-µ	0.38

3.2 Coupled solution method and time step verification

The transfer mechanisms of the unidirectional and bidirectional coupling algorithms are illustrated in Figure 7. As shown in the figure, the flow field and structural calculations adopt the same time step. Within each time step, Fluent and Abaqus respectively solve the flow and structural control equations, while MpCCI manages the coupling process and provides a data exchange platform. Aerodynamic loads obtained from the flow field calculation and displacement deformations from the structural analysis are exchanged through the coupling interface. The aerodynamic loads include pressure and viscous stress generated by the flow field. For the unidirectional coupling method, the time-domain coupling advancement process within the 0 to *t* time step is as follows for the unidirectional coupling method:

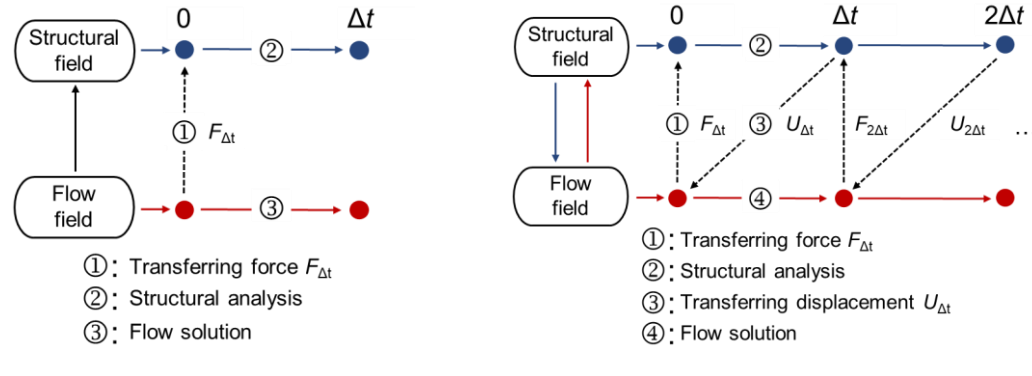
- 1.MpCCI extracts the aerodynamic loads on the coupling surface from the steady-state flow field computed by Fluent and applies them to the corresponding structural surface elements.
- 2. Abaqus performs transient structural analysis based on the applied aerodynamic loads, resulting in the deformation displacement distribution at time t.
- 3. Fluent completes the unsteady calculation based on the original flow field boundary to obtain the flow field at time *t*.

For the bidirectional coupling method, the time domain coupling process within the 0 to Δt time step is as follows:

- 1.MpCCI extracts the aerodynamic loads on the coupling surface from the steady-state flow field computed by Fluent and applies them to the corresponding structural surface elements.
- 2. Abaqus performs transient structural analysis based on the applied aerodynamic loads, resulting in the deformation displacement distribution at time t.
- 3.MpCCI extracts the deformation displacements on the coupling surface from the structural response characteristics obtained by Abaqus finite element analysis and transfers them to the corresponding flow field boundary grid, causing a change in the flow field boundary coordinates.
- 4.Fluent completes the unsteady calculation based on the new flow field boundary to obtain the flow field at time *t*.
- 5.Steps 2-4 are repeated within the Δt to $2\Delta t$ time steps, using the flow field distribution obtained from the 0 to Δt coupling calculation as the initial field value for this time step.

Due to the issues of time step lag and the non-conservation of energy on the coupling surface, the loosely fluid-structure interaction method based on the serial mechanism has first-order time

accuracy. Moreover, since the structural response time scale is larger than the flow time scale, the optimal time steps for the two physical fields are not consistent. Therefore, it is necessary to use a smaller coupling calculation time step to ensure computational accuracy and stability.



(a) Unidirectional FSI method

(b) Bidirectional FSI method

Figure 7 – Unidirectional/ Bidirectional fluid-structure interaction mechanism

The coupling time step has a significant influence on the efficiency and accuracy of fluid-structure interaction simulations. Sensitivity analysis of the coupling time step of the serpentine nozzle is conducted based on grid independence analysis. Three sets of different coupling time steps, $\Delta t = 1$ ms, $\Delta t = 2$ ms, and $\Delta t = 4$ ms, are selected here for fluid-structure interaction numerical calculations, with key variables being the wall static pressure and the structural deformation of the upper wall downstream of the first bend of the nozzle, as shown in Figure 8. It can be observed that the differences in wall static pressure distribution calculated using the three sets of coupling time steps mainly occur on the upper wall and downstream of the first bend. The maximum error in static pressure obtained from calculations with $\Delta t = 2$ ms and $\Delta t = 4$ ms reaches 7.85%; however, the static pressure distributions between $\Delta t = 1$ ms and $\Delta t = 2$ ms are essentially consistent. Therefore, using a coupling time step of $\Delta t = 2$ ms can effectively reduce computation time while accurately simulating the fluid-structure interaction characteristics of the serpentine nozzle.

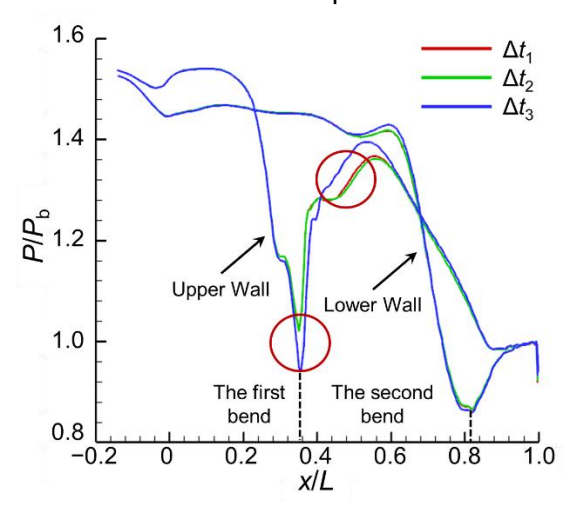


Figure 8 – Static pressure distribution based on asymmetrically long serpentine nozzle symmetric surface

3.3 Experimental instruments and measurement methods

To elucidate the deformation characteristics of key regions of the serpentine nozzle under fluid-structure interaction and to verify the accuracy of the unidirectional/bidirectional coupling methods, aerodynamic deformation experiments were conducted using a scaled-down model of a dual serpentine nozzle. The aerodynamic deformation experimental model of the serpentine nozzle includes an annular mixer model and a dual serpentine convergent nozzle model, as shown in Figure 9. This model is scaled down from the numerical computation model with a scale ratio of 10:1, constrained by experimental conditions. The structural material of the experimental model is SLA photopolymer resin, with material parameters listed in Table 4, and a wall thickness of 1.6 mm.

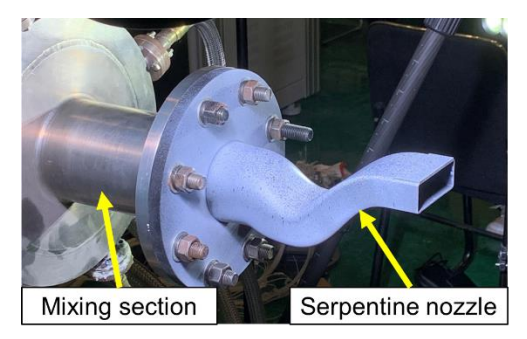


Figure 9 – Experimental model of aerodynamic deformation of double-ducted serpentine nozzle

Table 4 Material parameter values of serpentine nozzle experimental model

Material parameter	Numerical value
Elastic Modulus-E _s (GPa)	2.6
Density- ρ_s (kg/m ³)	1130
Poisson's ratio-μ _s	0.42

The experimental study on the aerodynamic deformation of the serpentine nozzle in this paper was conducted on the "Experimental Platform for the Integration of Dual Flowpath Exhaust System Thrust Vectoring and Infrared Radiation". The experimental platform primarily consists of a six-component force balance system, a primary flow system, a secondary flow system, an auxiliary flow system, and a flow field measurement system. To accurately describe the deformation characteristics of the serpentine nozzle, the VIC-3D (Video Image Correlation-3D) non-contact full-field strain analysis and measurement system was employed to obtain the deformation and displacement distribution at key locations on the nozzle wall. The core theory of the VIC-3D system is the Three-Dimensional Digital Speckle Correlation Method (3D-DSCM), which integrates the speckle correlation principle of the Two-Dimensional Digital Speckle Correlation Method (2D-DSCM) with the spatial imaging principle of binocular stereo vision. By comparing the three-dimensional images composed of random feature points on the object's surface before and after deformation, the system captures pixel-level displacements of feature points. It then solves for the object's surface displacement and strain distribution through grayscale search of the image correlation area. The VIC-3D system mainly comprises an optical measurement system and a software analysis system, as shown in Figure 10. The core equipment of the optical measurement system is two high-speed cameras. This system can provide full-field deformation shapes, displacement, and strain contour maps of the target object in three-dimensional space. The measurement accuracy for deformation displacement is 0.01 mm, and for strain, it is 0.005%.

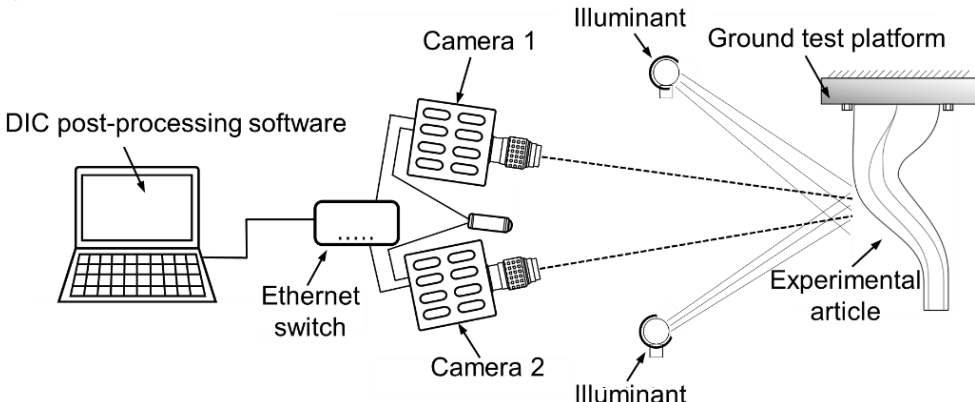


Figure 10 – VIC-3D (Video Image Correlation-3D) measurement and analysis system

4. Results

4.1 Serpentine nozzle unidirectional /bidirectional fluid-structure interaction characteristics

The serpentine nozzle configuration includes a high-curvature S-shaped bending channel and a round-to-square transition section, among other complex geometrical features. The high-curvature S-shaped and round-to-square geometrical configuration results in non-uniform flow field characteristics within the serpentine nozzle, creating a complex distribution of aerodynamic loads on

the wall surfaces. The internal flow field characteristics of the serpentine nozzle in the initial uncoupled state are shown in Figure 11. Additionally, the complex configuration of the serpentine nozzle enhances its structural elasticity, leading to significant deformation displacements. Non-uniform high-speed, high-pressure airflow applies rapidly changing aerodynamic loads to the elastic structure of the nozzle wall, resulting in deformation. The deformation displacements of the nozzle, in turn, are transmitted to the flow field boundaries, altering the internal and external flow characteristics. Consequently, the aerodynamic load distribution on the nozzle wall surfaces also changes. The flow field characteristics and the elastic structure of the serpentine nozzle iteratively exchange aerodynamic loads and deformation displacements in the time domain, ultimately forming a dynamic equilibrium under fluid-structure interaction.

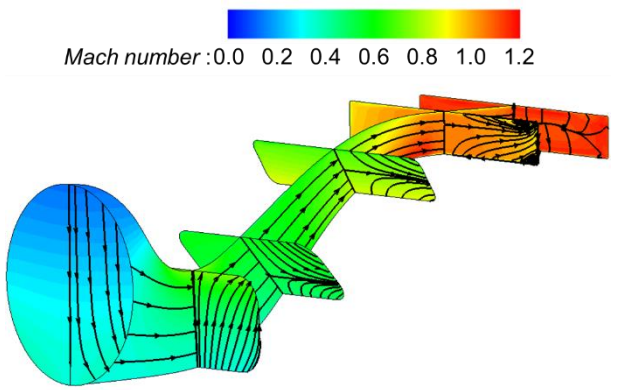
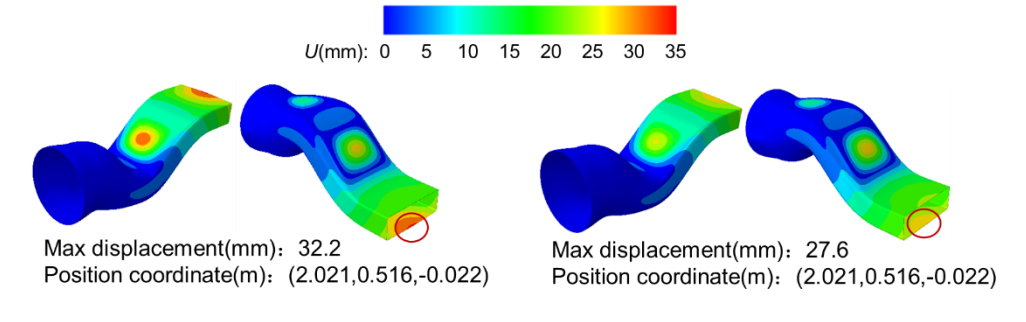


Figure 11 – Ma and streamline distributions inside serpentine nozzle at the initial uncoupled state The serpentine nozzle profile is transversely symmetric and bends along the longitudinal direction, leading to the primary deformation characteristics due to fluid-structure interaction occurring along the bending direction of the nozzle profile, i.e., along the Y-axis. The deformation displacement distributions under unidirectional and bidirectional fluid-structure interaction are shown in Figure 12. As can be seen from the figure, the deformation distribution trends of the serpentine nozzle are consistent under both unidirectional and bidirectional fluid-structure interactions, although the magnitudes of deformation differ. For both unidirectional and bidirectional coupling methods, the deformation characteristics of the serpentine nozzle structure are primarily located in the downstream section of the first S-bend channel and the central region of the nozzle exit. Excessive pressure loads cause the upper and lower walls in the middle region of the second bend channel to bulge outward. The serpentine bend configuration results in the static pressure on the lower wall being significantly lower than that on the upper wall at the turning point of the second bend and the straight section of the nozzle. Consequently, the nozzle structure in this region is subjected to an upward resultant force in the Y direction, leading to an overall upward bend of the nozzle exit section along the Y-axis, with the displacement of the upper wall being greater than that of the lower wall. The maximum deformation under both unidirectional and bidirectional fluid-structure interactions occurs at the center point of the upper wall at the nozzle exit. However, the overall deformation is greater under unidirectional coupling than under bidirectional coupling. The maximum deformation under unidirectional fluid-structure interaction is 32.2 mm, while the maximum deformation under bidirectional fluid-structure interaction is 27.6 mm.



(a) Unidirectional FSI method

(b) Bidirectional FSI method

Figure 12 – Displacement distribution under unidirectional/bidirectional fluid-structure interaction

To analyze the fluid-structure interaction characteristics of the serpentine nozzle more precisely,

here are the dimensionless axial positions along the nozzle cross-sections, as shown in Figure 13. In this study: Section A is the exit section of the mixer and the inlet section of the nozzle; Section B is located between the nozzle inlet and the first bend; Section C is located at the first bend; Section D is situated between the first bend and the second bend; Section E is located at the second bend; Section F is the inlet section of the constant straight section; Section G is the exit section of the nozzle.

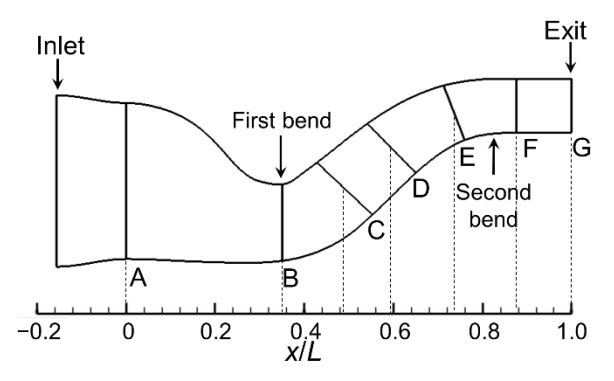


Figure 13 – The dimensionless axial positions along the nozzle cross-sections

Figure 14 and Figure 15 compares the Mach number distribution on the symmetrical surface and along the axial cross-sections of the serpentine nozzle under uncoupled and unidirectional/bidirectional coupling conditions. Combining with Figure 13, under unidirectional/bidirectional coupling conditions, the "bulging" of the wall surface near the center of the downstream channel of the first bend causes a local expansion-contraction feature in the nozzle passage in that region. After unidirectional/bidirectional coupling, the increased "bulging" on the upper wall surface of the first bend downstream increases the bending curvature of the upper wall surface in that region, leading to flow separation due to adverse pressure gradients. A small area of low-speed airflow appears on the upper side of section C, and this separated flow extends downstream to the nozzle exit. The "bulging" on the lower wall surface increases the curvature of the nozzle passage near the lower wall of the second bend, causing the airflow to accelerate drastically to supersonic speeds in that region. Furthermore, the turning speed under unidirectional fluid-structure interaction is significantly greater than that under bidirectional fluid-structure interaction, resulting in a noticeably larger range of localized high-speed airflow on the lower side of section E compared to the uncoupled state.

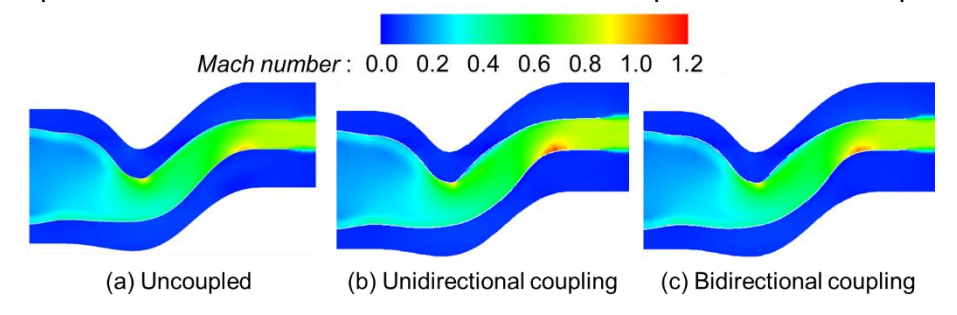


Figure 14 – Mach number distribution on symmetric surface of serpentine nozzle

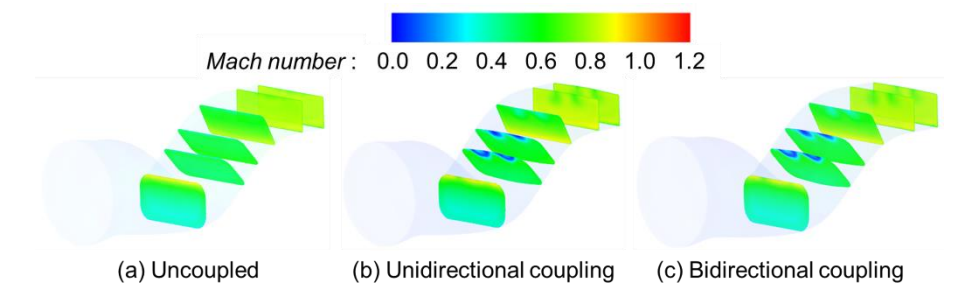
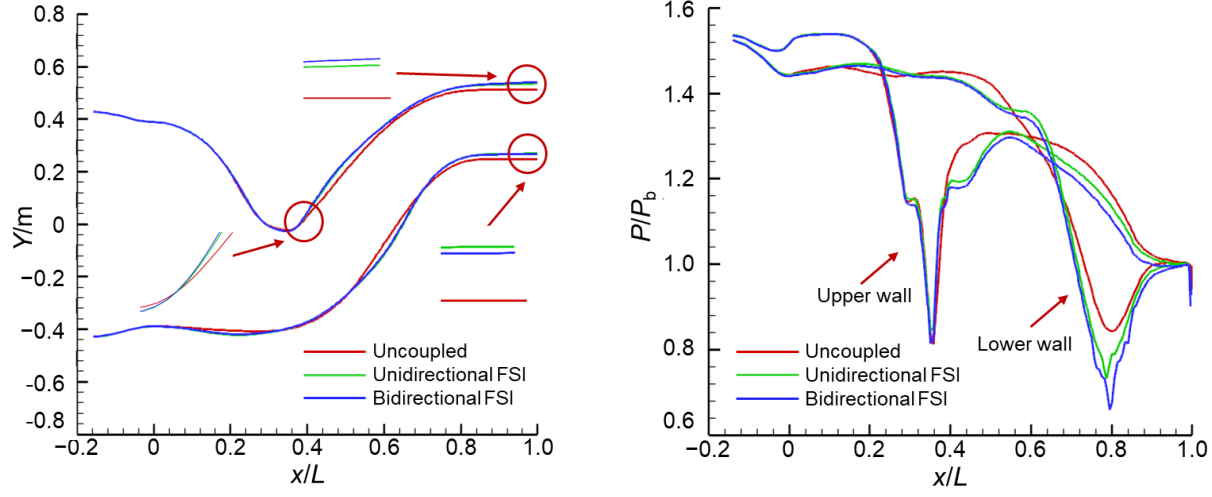


Figure 15 – Mach number distribution along section of serpentine nozzle

The geometric features and wall pressure distribution on the symmetrical surface of the serpentine nozzle under uncoupled and unidirectional/ bidirectional coupling conditions are illustrated in Figure 16. Combining Figures 16(a) and 16(b), the airflow separation region near the upper wall

downstream of the first bend causes a low-pressure zone to appear within the dimensionless position range of 0.4 to 0.6. Compared to the uncoupled state, the intense airflow acceleration near the second bend under unidirectional/bidirectional fluid-structure interaction significantly reduces the static pressure on the lower wall within the dimensionless position range of 0.7 to 0.8. Furthermore, the reduction magnitude under unidirectional coupling is greater than that under bidirectional coupling, resulting in greater deformation under unidirectional coupling than under bidirectional coupling. The "bulging" of the lower wall in the second S-bend channel causes pressure fluctuations on the lower wall within the dimensionless position range of 0.4 to 0.7.



- (a) Geometric characteristics of symmetrical wall surface of serpentine nozzle
- (b) Symmetrical wall pressure distribution of serpentine nozzle

Figure 16 – Symmetric surface geometric features and wall static pressure distribution of serpentine nozzle

Figure 17 depicts the velocity distribution along the centerline and symmetrical surface downstream of the serpentine nozzle outlet under uncoupled and unidirectional/bidirectional coupling conditions. It can be observed that the axial length of the jet flow remains essentially consistent across all three conditions, indicating minimal impact of deformation characteristics on the wetted perimeter area of the serpentine nozzle. The high-speed jet flow at the nozzle exit experiences little change in shear with the atmosphere. Combining Figure 16(a) with Figure 16(b), it is evident that under coupling conditions, the upward bending of the nozzle's straight section results in an increased Y-axis velocity of the jet flow. The jet flow deflects upward along the centerline downstream of the nozzle exit, with little difference observed between unidirectional and bidirectional coupling states.

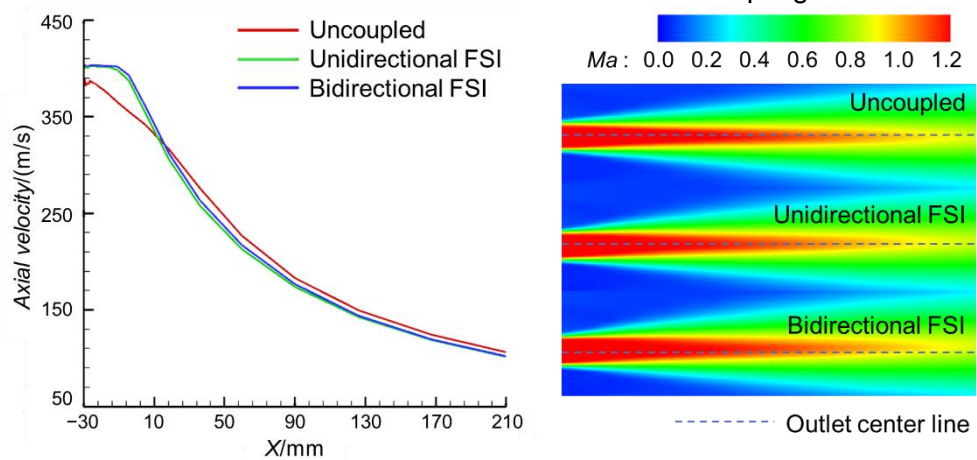


Figure 17 – Velocity distribution of nozzle outlet center line and symmetrical surface in uncoupled state and unidirectional/bidirectional coupling state

Table 5 compares the aerodynamic performance of the serpentine nozzle under uncoupled and unidirectional/bidirectional coupling conditions. It can be observed that for unidirectional coupling, the fluid-structure interaction effect results in a decrease in the total pressure recovery coefficient of

the serpentine nozzle by 1.2% and a decrease in the thrust coefficient by 0.5%. For bidirectional coupling, the fluid-structure interaction effect leads to a decrease in the total pressure recovery coefficient by 1.1% and a decrease in the thrust coefficient by 1.75%. Under unidirectional coupling conditions, the "bulging" of the wall surface in the second S-bend channel not only increases the wetted perimeter area and curvature of the nozzle profile, exacerbating friction and local losses but also induces flow separation downstream of the first bend, resulting in vortex losses. These flow losses collectively contribute to the decrease in the total pressure recovery coefficient of the serpentine nozzle. Additionally, the upward bending of the straight section increases the angle of the thrust vector along the Y-axis, leading to a decrease in axial thrust. Therefore, the thrust of the serpentine nozzle significantly decreases under unidirectional coupling conditions. Under bidirectional coupling conditions, due to the reduced overall deformation compared to unidirectional coupling, the flow losses caused by the wall "bulging" are smaller, resulting in a smaller change in the total pressure recovery coefficient compared to unidirectional coupling.

Coupling type	Total pressure recovery coefficient		thrust (N)		Thrust vector Angle(°)	
	Value	Rate	Value	Rate	Value	
Uncoupled	0.980		1908		0.016	
Unidirectional FSI	0.968	-1.2%	1898	-0.50%	1.02	

-1.1%

1875

-1.75%

0.9

Table 5 Comparison of aerodynamic performance of unidirectional/bidirectional FSI

4.2 Experimental study on structural deformation of serpentine nozzle

0.969

Bidirectional FSI

The experiment was conducted under ground conditions, and the pressure ratio at the outer duct inlet of the nozzle is SPR=1.60, and the pressure ratio at the core duct inlet is NPR=1.54. The measurement range mainly includes the upper and lower wall surfaces of the second section of the serpentine channel and the straight section of the nozzle. The wall deformation displacement distribution of the serpentine nozzle is shown in Figure 18. The results show that the maximum deformation displacement of the upper wall of the nozzle is located at the middle position of the nozzle outlet, and the maximum displacement value is 2.8mm. The deformation displacement of the lower wall of the nozzle shows a discontinuous distribution along the flow direction, and the main deformation characteristics are located at the center area of the first and second sections of the serpentine channel and the nozzle outlet. The maximum deformation displacement of the lower wall is also located at the middle position of the nozzle outlet, and the maximum displacement value is 2.9mm.

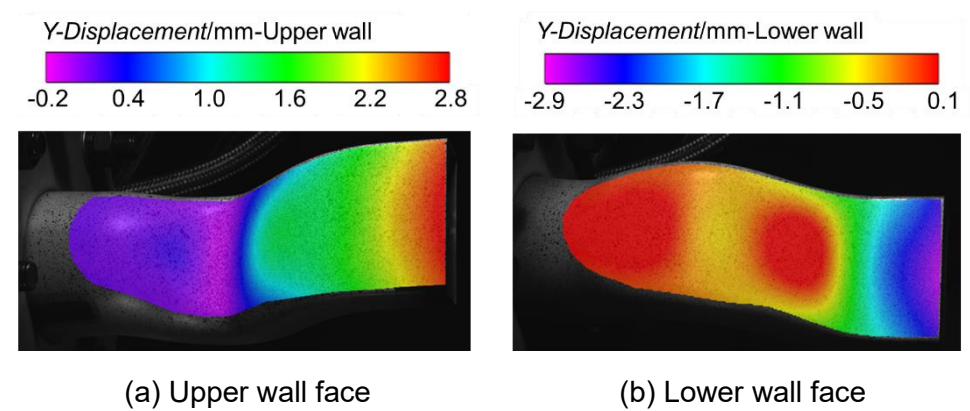


Figure 18 – Wall deformation and displacement distribution of serpentine nozzle

The wall deformation and displacement distribution of the symmetrical surface of the serpentine nozzle are shown in Figure 19. It can be seen from the figure that the pipeline structure downstream of the first bend (the second serpentine channel and the equal straight section) bends upward, so the deformation and displacement of the upper and lower walls of the equal straight section along the Y direction. The lower wall of the first section of serpentine channel and the central areas of the upper and lower walls of the second section of serpentine channel have local bulges, and the

deformation characteristics of the lower wall of the second section of serpentine channel are more prominent. Because the upper wall of the second serpentine channel is partially convex, the upper wall of the first bend is depressed along the Y direction.

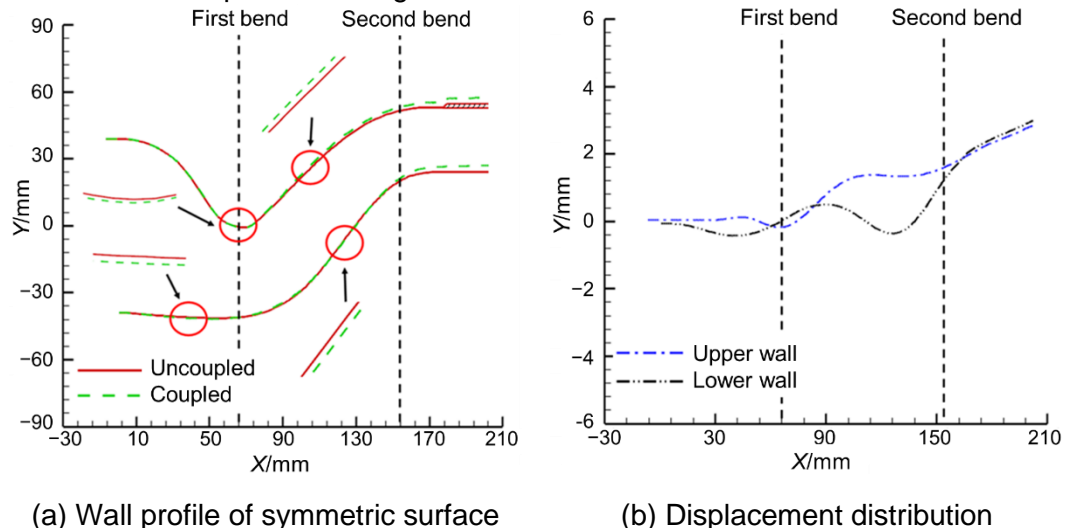


Figure 19 – Displacement distribution of wall deformation on the symmetrical surface

This study compares the key deformation characteristics predicted by unidirectional and bidirectional fluid-structure interaction (FSI) numerical simulations with experimental results. Figure 20 illustrates the deformation displacement distribution on the upper and lower walls of the serpentine nozzle. It is observed that the critical deformation features and their distribution locations obtained from both unidirectional and bidirectional FSI simulations align closely with the experimental results. These deformations are primarily manifested as local "bulging" in the downstream region of the first S-bend and upward displacement along the Y-axis at the straight section of the nozzle exit. However, there are discrepancies when compared to experimental results: for the unidirectional coupling method, the deformation in the bulging area downstream of the first bend and the upper wall at the exit is greater than the experimental measurements, while the deformation of the lower wall at the exit is smaller. For the bidirectional coupling method, the deformation downstream of the first bend and on the lower wall at the exit exceeds the experimental results, whereas the upper wall at the exit shows slightly less deformation than the experimental data.

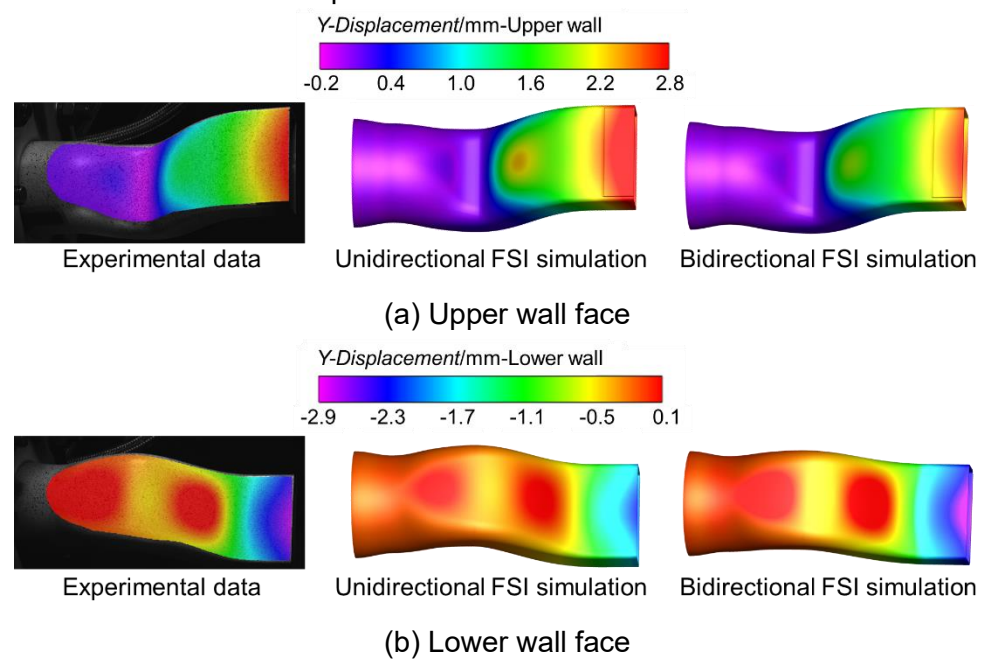


Figure 20 – Comparison between experimental data and numerical results of serpentine nozzle

Figure 21 compares the numerical results of the wall profile on the symmetry plane of the serpentine nozzle with the experimental data, and Table 6 presents the contour errors of the nozzle model's symmetry plane. From the results of Figure 21 and Table 6, it is evident that the regions with larger

errors are mainly located at the upper wall downstream of the first bend and at the nozzle exit. For the unidirectional coupling method, the maximum relative error on the upper wall downstream of the first bend is 15.6%, while the maximum relative errors at the upper and lower walls of the nozzle exit are 16.9% and 23.4%, respectively. For the bidirectional coupling method, the maximum relative error on the upper wall downstream of the first bend is 9.0%, and the maximum relative errors at the upper and lower walls of the nozzle exit are 9.1% and 8.8%, respectively. The reason for these discrepancies is that FSI calculations suppress the dynamic response of the nozzle structure, neglecting the structural deformation characteristics induced by vibration in the serpentine nozzle. In the case of unidirectional coupling, the lack of interaction between aerodynamic pressure and structural deformation further amplifies the errors in the calculations. Compared to numerical/experimental errors of different types of nozzles reported in the literature (average error of 20% in reference [14] and a minimum error of 7% in reference [15]), the bidirectional FSI numerical results are more reasonable and reliable.

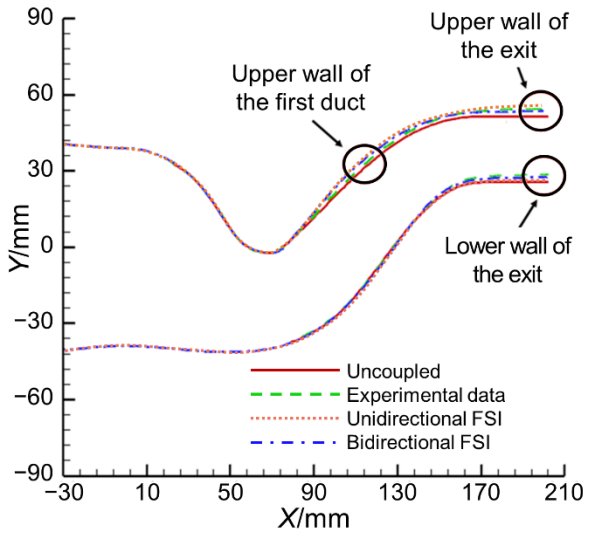


Figure 21 – Comparison between experimental data and numerical results of wall profile of symmetrical surface of serpentine nozzle

Table 6 Contour error values of symmetric surface

Deformation	Relative	Experimental	Unidirectional FSI		Bidirectional FSI	
position position x/L	position x/L	data /mm	Value/mm	Rate	Value/mm	Rate
First S-bend downstream	0.62	1.66	1.918	15.6%	1.809	9.0%
Upper exit wall	1	2.80	3.273	16.9%	2.545	9.1%
Lower exit wall	1	2.91	2.229	23.4%	3.166	8.8%

In summary, based on the experimental and numerical studies of the serpentine nozzle, the deformation characteristics of the serpentine nozzle under fluid-structure interaction primarily manifest as local bulging on the upper and lower walls of the first S-bend channel and upward bending along the Y-axis at the nozzle exit. Both unidirectional and bidirectional coupling methods accurately predict the deformation positions and trends. However, in quantitative analysis, the unidirectional coupling method exhibits larger errors, while the bidirectional fluid-structure interaction numerical method can accurately simulate the aerodynamic deformation characteristics of the turbofan engine serpentine nozzle. This method aligns more closely with the physical laws in real-world conditions, and thus, the bidirectional coupling method should be preferentially adopted in practical calculations.

5. Conclusions

This study investigates the aerodynamic deformation coupling characteristics of a serpentine nozzle using different fluid-structure interaction (FSI) methods, supplemented by experimental research on aerodynamic deformation. It compares and analyzes the structural deformation characteristics and

internal/external flow features of the serpentine nozzle under unidirectional and bidirectional FSI methods, verifying the accuracy of these methods against experimental results. The following conclusions are drawn:

- (1) The FSI effect induces structural deformation in the serpentine nozzle. The deformation distribution trends are consistent under both unidirectional and bidirectional FSI methods, with deformation areas located downstream of the first S-bend channel and at the center and exit of the nozzle. The maximum global deformation occurs at the center point of the upper wall at the nozzle exit. However, the overall deformation is greater in the unidirectional coupling method, with a maximum deformation of 32.2 mm, compared to 27.6 mm for the bidirectional coupling method.
- (2) The structural deformation of the serpentine nozzle significantly degrades its aerodynamic performance. The wall 'bulging' in the first S-bend channel exacerbates frictional and local losses, reducing the total pressure recovery coefficient. Additionally, the upward bending of the straight section increases the thrust vector angle along the Y-axis, significantly reducing the nozzle's thrust. For unidirectional coupling, the FSI effect decreases the total pressure recovery coefficient by 1.2% and the thrust coefficient by 0.5%. For bidirectional coupling, the FSI effect decreases the total pressure recovery coefficient by 1.1% and the thrust coefficient by 1.75%.
- (3) Based on the experimental and numerical studies, both unidirectional and bidirectional coupling methods accurately predict the deformation positions and trends of the serpentine nozzle. However, in quantitative analysis, the unidirectional coupling method exhibits larger errors, with a maximum error of 23.4%, while the bidirectional FSI numerical method shows a maximum error of 9.1%. The bidirectional FSI method can accurately simulate the aerodynamic deformation characteristics of the serpentine nozzle in a turbofan engine, aligning more closely with physical laws under real conditions. Therefore, the bidirectional coupling method should be preferred in practical computations.

6. Contact Author Email Address

mailto: zhouli@mail.nwpu.edu.cn

7. Copyright Statement

The authors confirm that they, and/or their company or organization, hold copyright on all of the original material included in this paper. The authors also confirm that they have obtained permission, from the copyright holder of any third-party material included in this paper, to publish it as part of their paper. The authors confirm that they give permission, or have obtained permission from the copyright holder of this paper, for the publication and distribution of this paper as part of the ICAS proceedings or as individual off-prints from the proceedings.

Acknowledgements

The authors would like to express their gratitude for the financial support of the National Natural Science Foundation of China (No. 52076180), Funds for Distinguished Young Scholars of Shaanxi Province (2021JC-10), National Science and Technology Major Project (J2019-II-0015-0036), Science Center for Gas Turbine Project (P2022-B-I-002-001, P2022-B-II-010-001), and the Fundamental Research Funds for the Central Universities.

References

- [1] Luo P, Zheng M. Thermal-Fluid-Solid Coupling Analysis of Aero-Engine Nozzle[J]. *Journal of Aerospace Science and Technology*, 2016, 4(4): 85-96.
- [2] Crowe D S, Martin C L. Effect of geometry on exit temperature from serpentine exhaust nozzles[C]//53rd AIAA Aerospace Sciences Meeting. 2015: 1670.
- [3] Dalenbring M, Smith J. Simulation of s-Duct dynamics using fluid-structure coupled CFD[C]//24th AIAA Applied Aerodynamics Conference. 2006: 2981.
- [4] Dalenbring M. Analysis of Materials and Structures used within the FoT25 Project Propulsion Integration[M]. System technology, Swedish defence research agency (FOI), 2006.
- [5] Liu C F, Qiu J. Aeroelasticity of Fluid-Structure Interaction Analysis Method [M]. Beijing: Beihang University Press, 2016.
- [6] Ye Z Y, Zhang W W, Shi A M. *Fluid-structure interaction mechanics and its application* [M]. Harbin: Harbin Institute of Technology Press, 2010.
- [7] Jaiman R, Geubelle P, Loth E et al. Transient Fluid–Structure Interaction with Non-Matching Spatial and Temporal Discretizations[J]. *Computers & Fluids*, 2011, 50(1): 120–135.
- [8] Piperno S, Farhat C. Partitioned procedures for the transient solution of coupled aeroelastic problems—Part II: energy transfer analysis and three-dimensional applications[J]. *Computer methods in applied mechanics and engineering*, 2001, 190(24-25): 3147-3170.
- [9] Urbanczyk P S, Alonso J J, Nigam N, et al. Coupled Multiphysics Analysis for Design of Advanced Exhaust Systems[C]//58th AIAA/ASCE/AHS/ASC Structures, Structural Dynamics, and Materials Conference. 2017: 0799.
- [10]Nigam N, Ayyalasomayajula S K, Tang Y, et al. Design Optimization of Advanced Exhaust Systems[C]//18th AIAA/ISSMO Multidisciplinary Analysis and Optimization Conference. 2017: 3331.
- [11]Smith J, Dalenbring M. Aeroelastic simulation of S-duct dynamics using structure-coupled CFD[C]//ICAS. 2006.
- [12]Sun P, Zhou L, Wang Z X, et al. Fluid-Structure Interaction Study of the Serpentine Nozzle for Turbofan[J]. *Journal of Applied Fluid Mechanics*, 2022, 15(5): 1563-1580.
- [13]Lee C, Boedicker C. Subsonic diffuser design and performance for advanced fighter aircraft[C]//Aircraft design systems and operations meeting. 1985: 3073..
- [14] Aghababaie A, Taylor N. Modelling side loads in separated rocket nozzles [C]//47th AIAA/ASME/SAE/ASEE Joint Propulsion Conference & Exhibit. 2011: 5687.
- [15]Brown A, Ruf J, McDaniels D. Recovering aerodynamic side loads on rocket nozzles using quasi-static strain-gage measurements[C]//50th AIAA/ASME/ASCE/AHS/ASC Structures, Structural Dynamics, and Materials Conference 17th AIAA/ASME/AHS Adaptive Structures Conference 11th AIAA No. 2009: 2681.